J. Biochem. **127**, 337–343 (2000)

Cocrystallization of a Mutant Aspartate Aminotransferase with a C5-Dicarboxylic Substrate Analog: Structural Comparison with the Enzyme–C4-Dicarboxylic Analog Complex[1]

Shinya Oue,[2] Akihiro Okamoto, Takato Yano, and Hiroyuki Kagamiyama[3]

Department of Biochemistry, Osaka Medical College 2-7 Daigakumachi, Takatsuki, Osaka 569-8686

Received October 4, 1999; accepted November 30, 1999

A mutant *Escherichia coil* aspartate aminotransferase with 17 amino acid substitutions (ATB17), previously created by directed evolution, shows increased activity for β-branched amino acids and decreased activity for the native substrates, aspartate and glutamate. A new mutant (ATBSN) was generated by changing two of the 17 mutated residues back to the original ones. ATBSN recovered the activities for aspartate and glutamate to the level of the wild-type enzyme while maintaining the enhanced activity of ATB17 for the other amino acid substrates. The absorption spectrum of the bound coenzyme, pyridoxal 5′-phosphate, also returned to the original state. ATBSN shows significantly increased affinity for substrate analogs including succinate and glutarate, analogs of aspartate and glutamate, respectively. Hence, we could cocrystallize ATBSN with succinate or glutarate, and the structures show how the enzyme can bind two kinds of dicarboxylic substrates with different chain lengths. The present results may also provide an insight into the long-standing controversies regarding the mode of binding of glutamate to the wild-type enzyme.

Key words: aspartate aminotransferase, crystallography, directed evolution, substrate specificity.

Aspartate aminotransferase (AspAT) catalyzes a reversible amino-group transfer between two acidic amino acids, aspartate and glutamate, and plays central roles in amino acid metabolism in a wide variety of organisms, from bacteria to mammals (*1–3*). A detailed reaction mechanism has been proposed based on the three-dimensional structure of the active site (*4*). The role of each active site residue in the catalytic process has been examined through site-directed mutagenesis studies on the *Escherichia coli* AspAT (*5–11*). X-ray crystallographic studies have also shown that substrate binding induces structural changes, from an "open" form to a "closed" form, in the gross conformation of this enzyme (*12–17*). Most of the above findings are, however, based on the results of functional and structural studies involving aspartate analogs such as 2-methyl-aspartate and maleate, whereas how AspAT binds glutamate or whether the detailed mechanism proposed for the reaction with aspartate holds for the reaction with glutamate has been controversial. As for the mode of binding of glutamate to AspAT, some reports have shown that glutamate-binding causes conformational changes to a closed form (*18–20*), and another that the enzyme structure remains in an open form after binding glutamate (*21*). This is mainly because the affinity of AspAT for the C5-dicarboxylic ligands is lower by >10-fold than that for the C4-dicarboxylic ligands, and hence one cannot cocrystallize AspAT with glutamate analogs. Although several attempts have been made to settle this issue, the results have remained inconclusive (*18–21*).

Recently, we reported a mutant *E. coli* AspAT with 17 amino acid substitutions (ATB17) created by directed evolution, which shows a 10^6-fold increase and a 100-fold decrease in catalytic efficiency for β-branched amino acids and acidic amino acids, respectively (*22, 23*). This mutant enzyme also shows enhanced activity for the other amino acid substrates. A series of mutant AspATs was constructed to study how the mutated residues affect the substrate specificity. One of the mutants, named ATBSN, in which Gly139 and Thr142 of ATB17 were mutated back to the wild-type residues, Ser and Asn, respectively, recovered the activity for acidic substrates while maintaining the enhanced activity for other amino acids. As a result, we unexpectedly obtained an aspartate aminotransferase with a broad substrate specificity. Compared to the wild-type AspAT (WT), ATBSN also shows increased affinity for substrate analogs including a glutamate analog, glutarate. We thus could determine the three-dimensional structure of ATBSN complexed with glutarate, together with the structure complexed with an aspartate analog, succinate. These structures show how the active site of an enzyme can accommodate two kids of dicarboxylic substrates with different chain lengths and may provide clues for modeling

[1] This work was supported by the Ministry of Education, Science, Sports and Culture of Japan (to T.Y.), and the Japan Society for the Promotion of Science ("Research for the Future" Program (to H.K.)).
[2] Present address: Department of Pediatrics, Osaka Medical College, 2-7 Daigakumachi, Takatsuki, Osaka 569-8686.
[3] To whom correspondence should be addressed. Fax: +81-726-84-6516, E-mail: med001@art.osaka-med.ac.jp
Abbreviations: AspAT, aspartate aminotransferase; PLP, pyridoxal 5′-phosphate; PMP, pyridoxamine 5′-phosphate.

how the wild-type enzyme binds the C5-dicarboxylic substrates.

MATERIALS AND METHODS

Materials—Pipes and Hepes were obtained from Dojindo Laboratories (Kumamoto). Glutaric acid, succinic acid, and maleic acid were from Nacalai Tesque (Kyoto). Isovaleric acid, α-ketovaleric acid, DL-α-keto-β-methyl-*n*-valeric acid, and α-ketoisocapronic acid were from Sigma (St. Louis). An *aspC*-deficient *E. coli* strain, TY103 (*24*), was used to express mutant AspATs.

Preparation of AspATs—Site-derected mutagenesis was performed on the single-stranded DNA of the ATB17 gene (*23*) subcloned into pUC118 using the "Sculptor" *in vitro* mutagenesis system (Amersham Pharmacia Biotech). The following synthetic oligonucleotide was used to direct the mutations (asterisks indicate the mismatches): 5′-GCT-CTT-ATG-GT*T-CGG-CCA-GCC-AGC-T*TG-GGT-TGC-TC-3′. The expression and purification of AspATs were performed as reported previously (*9*). @ @ @ @

Activity Measurement of AspATs—The overall transamination reaction catalyzed by this enzyme is:

L-aspartate + 2-oxoglutarate ⇌ oxalacetate + L-glutamate (Eq. 1).

This overall transamination reaction consists of two half-transamination reactions (*25*):

EL + Asp ⇌ EL · Asp ⇌ EM · OA ⇌ EM + OA (Eq. 2a)

EL + Glu ⇌ EL · Glu ⇌ EM · OG ⇌ EM + OG (Eq. 2b)

where EL and EM denote the pyridoxal 5′-phosphate (PLP) form and pyridoxamine 5′-phosphate (PMP) form enzymes, respectively; and Asp, OA, Glu, and OG are aspartate, oxalacetate, glutamate, and 2-oxoglutarate, respectively.

The activity of AspATs for each substrate, except for that of WT for valine or isoleucine, was measured by spectrophotometrically monitoring single turnovers of the half reactions with various concentrations of the substrate using an Applied Photophysics stopped-flow apparatus (modex SX. 17MV) as described (*25*). The activity of WT for valine or isoleucine was measured using a Hitachi spectrophotometer U-3300. The reactions were performed at 25°C in a buffer system comprising 50 mM Hepes, pH 8.0, containing 0.1 M KCl and 10 μM EDTA, at a protein concentration of 20 μM.

Measurement of the K_d Values for Analogs—The dissociation constants of AspATs for maleate, succinate, glutarate, and isovalerate were determined by spectrophotometric titration (*26*, *27*). The spectral changes were measured using a Hitachi spectrophotometer U-3300 in 50 mM Hepes, pH 8.0, containing 0.1 M KCl and 10 μM EDTA at 25°C.

Crystallography—The crystals of ATBSN complexed with succinate or glutarate were grown by the sitting drop vapor diffusion method. Three-microliter drops containing 37 mg/ml protein were mixed with 1 μl of 1 M sodium succinate (or sodium glutarate) and 3 μl of a reservoir solution containing 1.7 M ammonium sulfate and 0.1 M Hepes, pH 7.5. The drops were equilibrated against 0.5 ml of the reservoir solution at 20°C. An X-ray data set was collected with a Rigaku R-AXIS IIc image plate detector mounted on a Rigaku RU-200 rotating anode generator operated at 40 kV and 100 mA with monochromatized CuK_α radiation at room temperature. The oscillation images were processed and reduced using the data processing software Rigaku PROCESS (*28*). Refinement of the structure began with the structure of the ATB17-isovalerate complex (*23*) as an initial model using X-PLOR 3.851 (*29*) with parameters derived by Engh and Huber (*30*). After conventional positional refinement, simulated annealing using the slow cool protocol was performed. The models were improved by conventional positional refinement and isotropic *B*-factor refinement, and manual rebuilding using Xfit (*31*) on the omit map was calculated with the coefficients $|F_O| - |F_C|$. After the *R*-factors had been adequately lowered, water molecules were added to the models and the structures were further refined. The coordinates have been deposited in the Protein Data Bank (code 1CZC or 1CZE for the ATBSN-Glutarate or ATBSN-Succinate complex, respectively).

RESULTS

Enzymatic Activity of AspATs—The kinetic parameters for β-branched and acidic substrates are shown in Table I. The k_{cat}/K_m values of ATBSN for β-branched substrates are slightly smaller than those of ATB17: 5.1- or 18-fold for valine or 2-oxovaline; 3.2- or 15-fold for isoleucine or 2-oxo-isoleucine, respectively. On the other hand, the k_{cat}/K_m values of ATBSN for glutamate and 2-oxoglutarate are increased 60- and 80-fold, respectively, compared to those of ATB17, and are almost comparable to those of WT. The K_m values of ATBSN for glutamate and 2-oxoglutarate are

TABLE I. **Kinetic parameters of AspATs for branched and acidic substrates.**

Substrate	WT[a]			ATB17[b]			ATBSN		
	k_{cat} (s^{-1})	K_m (mM)	k_{cat}/K_m ($s^{-1}\cdot M^{-1}$)	k_{cat} (s^{-1})	K_m (mM)	k_{cat}/K_m ($s^{-1}\cdot M^{-1}$)	k_{cat} (s^{-1})	K_m (mM)	k_{cat}/K_m ($s^{-1}\cdot M^{-1}$)
L-Valine	—[c]	—[c]	$3.4(0.16)\times10^{-3}$	12	5.5	2.1×10^{3}	28 (1)	68 (5)	410
L-Isoleucine	—[c]	—[c]	$4.9(0.024)\times10^{-4}$	8.4	140	60	5.0 (0.2)	270 (10)	19
2-Oxovaline[d]	5.7×10^{-3}	100	0.057	90	2.4	3.8×10^{4}	23 (2)	11 (1)	2.1×10^{3}
2-Oxoisoleucine[d]	3.3×10^{-3}	52	0.063	250	7.3	3.4×10^{4}	29 (3)	13 (2)	2.2×10^{3}
L-Aspartate	550	4.5	1.2×10^{5}	—	—	3.3×10^{3}	—[e]	—[e]	—[e]
L-Glutamate	700	38	1.8×10^{4}	—	—	570	260 (60)	7.7 (2.0)	3.4×10^{4}
Oxalacetate	800	0.035	2.3×10^{7}	120	2.2	5.5×10^{4}	—[e]	—[e]	—[e]
2-Oxoglutarate	600	1.3	4.6×10^{5}	—	—	2200	12 (0.3)	0.068 (0.04)	1.8×10^{5}

Standard deviations are given in parentheses. [a]Data from Ref. *25*, except for those for branched-chain 2-oxo acids (*22*). The parameters for valine and isoleucine were reexamined in this study. [b]Data from Ref. *23*. [c]Reactions did not show stauration kinetics with the substrate concentrations examined. [d]Abbreviations: 2-oxovaline, 2-ketoisovaleric acid; 2-oxoisoleucine, DL-2-keto-3-methyl-*n*-valeric acid. [e]Parameters could not be determined experimentally (see text).

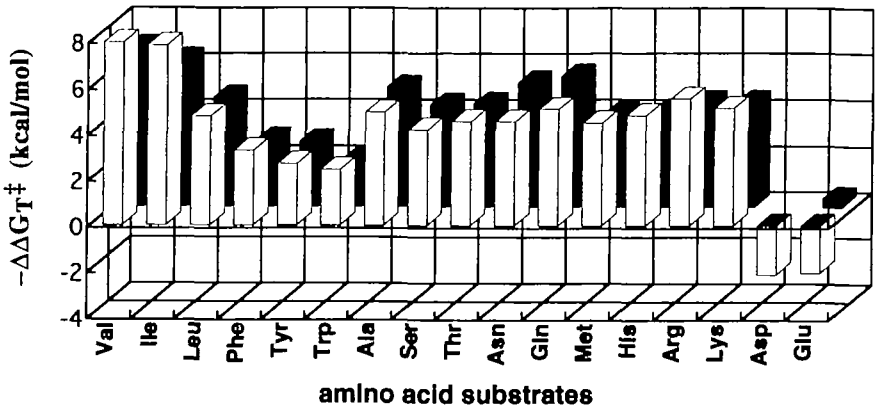

Fig. 1. **Stabilization of the activation free energy for various amino acid substrates by ATB17 (white) or ATBSN (gray) relative to WT.** $-\Delta\Delta G_T^{\ddagger} = [RT\{(k_{cat}/K_m)_X/(k_{cat}/K_m)_{WT}\}]$. Positive bars indicate that the catalytic efficiency of a mutant enzyme, X, is higher than that of the wide-type AspAT, and negative bars indicate *vice versa*. The value of ATBSN for aspartate is not indicated because it could not be determined (see text).

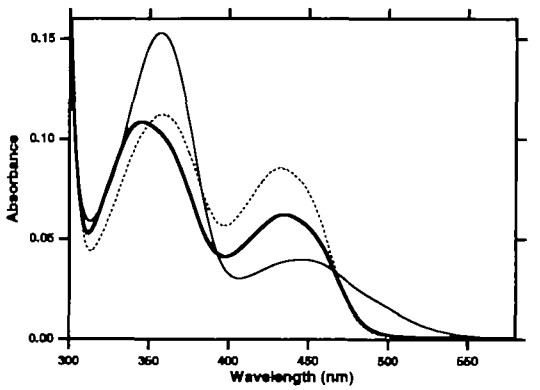

Fig. 2. **Absorption spectra of AspATs.** Absorption spectra of the wild-type AspAT (dotted line), ATB17 (thin line), and ATBSN (thick line) are presented. All of the spectra were measured in a 50 mM Pipes buffer, pH 6.5, at a protein concentration of 19 mM.

smaller than those of WT.

The k_{app} values of ATBSN for aspartate were dependent on the aspartate concentration: k_{app}= 30–500 s^{-1} for 0.1–2 mM aspartate. To determine the k_{cat} and K_m values for aspartate, each k_{app} value has to be corrected for the contribution of the reverse reaction, that is, the reaction of the PMP-form enzyme with oxalacetate (Eq. 2a) (*25*). The k_{app} value was, however, constant (about 7 s^{-1}) in the range of 0.05–1 mM oxalacetate, implying that the K_m value of ATBSN for oxalacetate is << 50 μM, which is too small to be determined. Because the kinetic parameters of ATBSN for oxalacetate could not be determined, the contribution of the reverse reaction could not be estimated. Thus we studied the overall-transamination reaction of ATBSN with aspartate and 2-oxovaline, where oxalacetate is eliminated from the reaction mixture by coupling the malate dehydrogenase reaction (*32*). The k_{cat}/K_m value for a substrate obtained from the overall reaction should be the same as that obtained from the half reaction (*25*). The k_{cat} value obtained from the overall reaction was, however, 0.3 s^{-1}, which is far smaller than the value estimated from the rate constants for the half reactions with aspartate and 2-oxovaline (k_{app} for aspartate, 30–500 s^{-1}; k_{cat} for 2-oxovaline, 23 s^{-1}). This indicates that the rate-limiting step of the overall reaction is different from that of the half reaction. Accordingly, the kinetic parameters could not be determined for aspartate and oxalacetate.

TABLE II. **Dissociation constants (mM) of AspATs.**

	WT	ATB17	ATBSN
Maleate	10[a]	>150[c]	0.77 (0.009)
Succinate	74[a]	—[d]	2.4 (0.03)
Glutarate	150[b]	>150[c]	1.5 (0.03)
Isovalerate	—[d]	5.5[e]	36 (3)

Standard deviations are given in parentheses. [a]Taken from Ref. *25*. [b]Taken from Ref. *24*. [c]Spectral changes did not show saturation in the range of analog concentrations, 5–100 mM. [d]No spectral changes were observed. [e]Taken from Ref. *23*.

The catalytic efficiencies (k_{cat}/K_m values) of ATB17 and ATBSN for various amino acid substrates were compared to those of WT. As shown in Fig. 1, the catalytic efficiency of ATBSN for glutamate recovered to the level of WT with maintenance of the high catalytic competence of ATB17 for other amino acid substrates.

Absorption Spectra of AspATs—The absorption spectra of WT, ATB17, and ATBSN were recorded in 50 mM Pipes, pH 6.5 (Fig. 2). WT gives two absorption bands at 358 and 430 nm that represent the deprotonated and protonated forms, respectively, of the imine nitrogen of the Schiff base formed between PLP and Lys258 (*33, 34*). As reported previously (*23*), the latter band of ATB17 is red-shifted to 450 nm and has a broad shoulder above 500 nm, although it remains to be determined what kind of molecular species corresponds to the shoulder. This shoulder completely disappeared in the case of ATBSN.

Dissociation Constants of AspATs for Substrate Analogs—The K_d values of AspATs for amino-group-free analogs are shown in Table II. ATB17 shows a remarkably increased affinity for a valine analog, isovalerate, whereas the affinity for dicarboxylic analogs is decreased. ATBSN shows higher affinity than WT for all the analogs. Compared to the K_d values of WT, those of ATBSN for aspartate analogs, maleate and succinate, are decreased 13- and 30-fold, respectively, and that for a glutamate analog, glutarate, is decreased 100-fold.

Overall Structures of AspATs—Among the enzyme-analog combinations shown in Table II, only the structures of the WT-maleate and ATB17-isovalerate complexes have been determined so far (*14, 23*). WT and ATB17 cannot be cocrystallized with other analogs. ATBSN could be cocrystallized with succinate and glutarate but not with isovalerate. Succinate, not maleate, was chosen as an aspartate analog because the structure of AspAT complexed with succinate has never been solved and also because succinate is

more suitable as a C4 analog when the structure of the complex is compared to that of the enzyme-glutarate complex.

The X-ray crystal structure of ATBSN complexed with glutarate or succinate was solved at 2.5- or 2.4-Å resolution, respectively (Table III). Figure 3 shows a comparison of the gross structures of the ATBSN-glutarate complex and the ATB17-isovalerate complex. The structure of the ATBSN-succinate complex is not shown because it is almost identical to that of the ATBSN-glutarate complex.

Upon binding the substrate, the small domain (residues 5 to 47 and 326 to 409: thick line in Fig. 3) of AspAT moves closer to the active site and the structure changes from an open form to a closed form (*15, 16*). When the large domain (residues 48 to 325; thin line in Fig. 3) of one subunit of the ATBSN-glutarate complex is superimposed on that of the ATB17-isovalerate complex, two features are evident: First, the ATBSN-glutarate complex is in the closed form, although less closed compared to that of the ATB17-isovalerate complex. Second, the large domains of the other subunit overlap each other poorly. The latter finding indicates that the spacial arrangement of the two subunits is altered between the two structures. The structure of the ATBSN-glutarate complex is similar to that of the WT-maleate complex.

Active-Site Structures of AspATs—The active-site structures of AspATs complexed with substrate analogs are shown in Fig. 4. The active site of the ATB17-isovalerate complex (*23* and also see Fig. 4A) was changed significantly from that of the WT-maleate complex: Arg292, which interacts with the side-chain carboxylate group of asparate, flips outside to the solvent; the tilt of the PLP molecule is changed because the side-chain indole ring of Trp140 is moved against the pyridine ring of PLP. Trp140 of ATB17 is also shifted toward the "bottom" of the active site. In the ATBSN-glutarate complex, the side chains of Arg292 and Trp140 are reoriented to the same positions as those in the WT-maleate complex. The side chain of Arg292 interacts with a carboxylate group, which corresponds to the side-chain carboxylate group of glutamate in an "end-on" symmetric geometry. Trp140 is moved so that the nitrogen of the indole ring can form a hydrogen bond with the side-chain carboxylate group of glutarate, as in the case of the WT-maleate complex. The active-site structure of the ATBSN-succinate complex is almost identical to that of the WT-maleate complex except for Met37, which is substituted for Ile in ATBSN (Fig. 4B). The active-site structure of the ATBSN-glutarate complex was compared to that of the ATBSN-succinate complex (Fig. 4C). The orientation of Arg292 and Arg386 is almost identical in the two structures, although the distance between the two guanidinium groups is slightly greater in the ATBSN-glutarate complex. The position of the C(3) atom of glutarate deviates significantly from that of succinate to maintain the distance between the two carboxylate groups. As a result, the orientation of the carboxylate group interacting with the Arg292 side chain differs between the two structures. The C(2) atom of each dicarboxylic analog, which corresponds to Cα of the amino acid substrate, is located at a position that would enable the amino group of the substrate to form an external Schiff base with PLP. Thus, these structures would correctly reflect the productive Michaelis complex of ATBSN with each corresponding substrate.

TABLE III. **Summary of the X-ray data collection and crystal data.**

	ATBSN with glutarate	ATBSN with succinate
Diffraction data		
Space group	$C222_1$	$C222_1$
Unit cell dimensions		
a (Å)	156.35	156.64
b (Å)	85.02	85.06
c (Å)	78.27	78.30
Total reflections	61,781	71,147
Unique reflections	16,658	18,949
Completeness (%)	98.8	99.7
Resolution range (Å)	75.0–2.5	75.0–2.4
R_{merge} (%)[a]	5.36	6.43
Refinement statics		
Resolution range (Å)	10.0–2.5	10.0–2.4
Number of reflections	16,330	18,622
Number of protein atoms	3,096	3,095
Number of water molecules	160	103
$R_{crystal}$ (%)[b]	18.8	19.5
R_{free} (%)[c]	24.3	24.4
Deviations from ideal geometry (rms)		
Bond lengths (Å)	0.008	0.008
Bond angles (°)	1.4	1.4
Improper angles (°)	1.28	1.26
Dihedrals (°)	23.7	23.8

[a] $R_{merge} = \Sigma_i |I_i - \langle I_i \rangle| / \Sigma_i \langle I_i \rangle$ where I_i is the intensity of an individual reflection and $\langle I_i \rangle$ is the mean intensity of that reflection. [b] $R_{cryst} = 100 \times \Sigma ||F_{obs}| - |F_{calc}|| / \Sigma |F_{obs}|$, where F_{obs} and F_{calc} are the observed and calculated structure factors, respectively. [c] R_{free} is calculated in the same manner as R_{cryst} with 10% of random reflections excluded from the refinement.

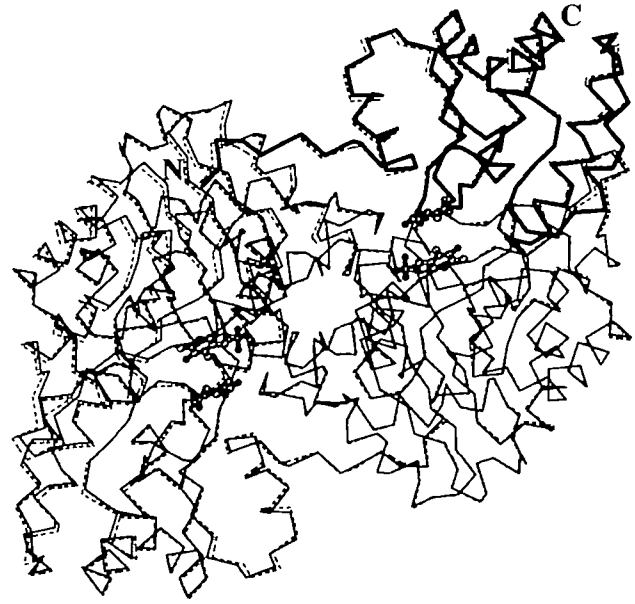

Fig. 3. **Superposition of the ATBSN-glutaratre complex (solid line) and ATB17-isovalerate complex (dotted line).** The large domain (residues 49–325) of one subunit of ATBSN was superimposed on the corresponding domain of ATB17. The small domain (the remaining residues) of the subunit of ATBSN is indicated by thick lines. The NH_2- and COOH-terminals of the subunit are indicated, N and C.

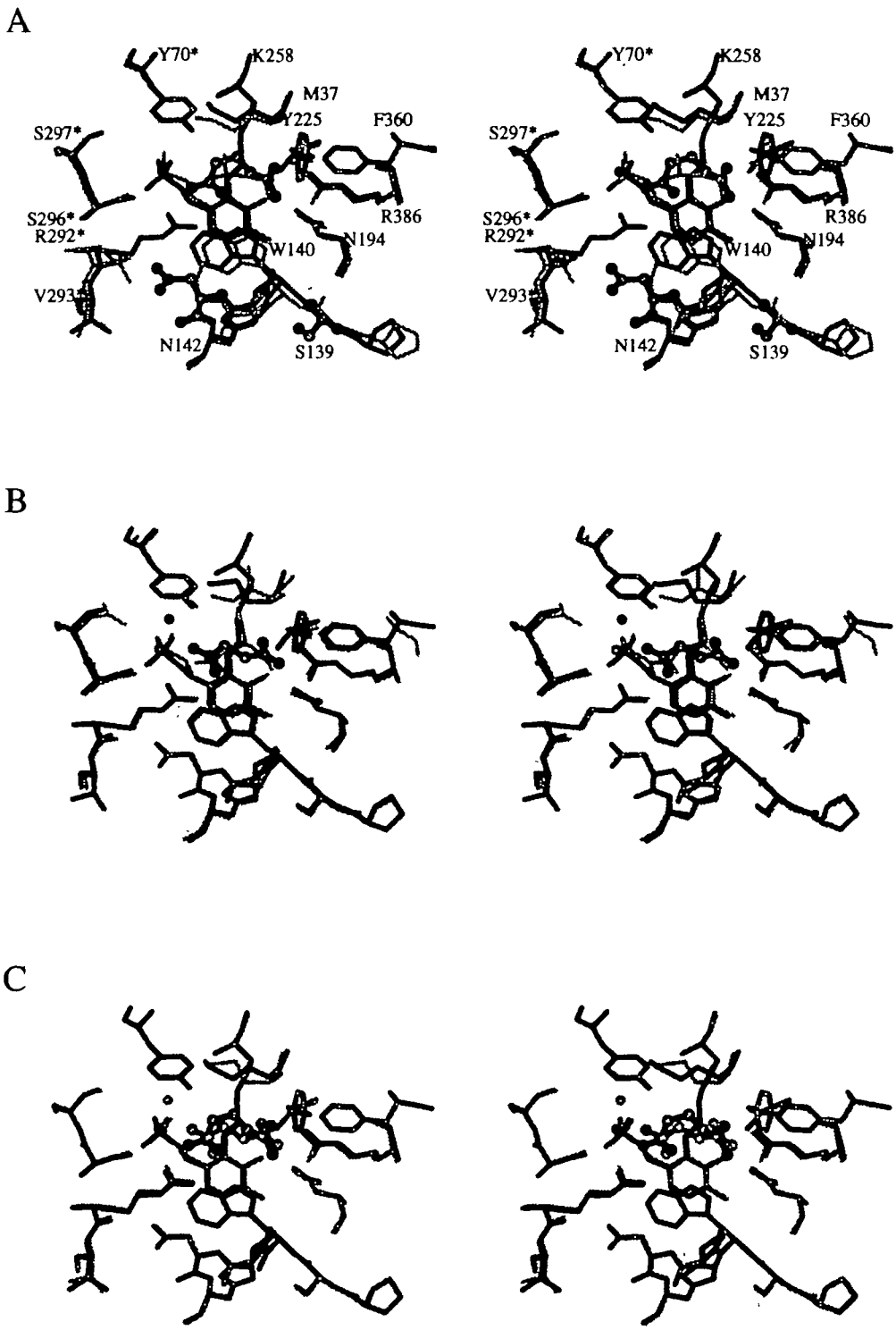

Fig. 4. **Close-up view of the active site of AspATs.** Comparison of the active-site structures between (A) the ATBSN-glutarate (dark line) and ATB17-isovalerate (faint) complexes, (B) the ATBSN-succinate (dark) and WT-maleate (faint) complexes, and (C) the ATBSN-glutarate (dark) and ATBSN-succinate (faint) complexes. The amino acid residues indicated by asterisks belong to the other subunit. Ile37, Ala293, and Asn297 are replaced by Met, Val, and Ser, respectively, in ATB17 and ATBSN. Ser139 and Asn142 are replaced by Gly and Thr, respectively, in ATB17.

DISCUSSION

Effects of Gly139 and Thr142 on the Substrate Specificity and Active-Site Structure of ATB17—As described previously (*23*), when the active-site structure of the ATB17-isovalerate complex was compared to that of the WT-maleate complex, the largest deviations in the backbone structure were observed at the "bottom" of the active site, especially around the Pro138–Thr142 loop. The two mu-tated residues, Gly139 and Thr142 in ATB17, are located in the Pro138–Thr142 loop. This loop contains Trp140, of which the indole ring stacks against the pyridine ring of PLP and is thought to adjust the tilt of PLP during the course of the catalytic process (*4*). These two residues were mutated in all the mutant enzymes obtained by directed evolution (*22*,

23), indicating that Ser139 and Asn142 are important for the increased catalytic efficiency for β-branched amino acids. Therefore, ATBSN was constructed, and its enzymatic properties and three-dimensional structure were analyzed to investigate the effects of these two mutations on the active-site structure and substrate specificity.

The active-site structure of ATBSN complexed with succinate or glutarate (Fig. 4) shows that the Pro138–Asn142 loop and the indole ring of Trp140 are reoriented to the same positions as that of the WT-maleate complex. The conformation of the flexible side chain of Met37, the only substitution found in the substrate binding site, is changed depending on the bound analogs. In the ATB17-isovalerate complex, the side chain of Arg292 protrudes into the solvent (23), while the side chain of Arg292 in the WT-maleate and ATBSN-succinate/glutarate complexes flips toward the active site and interacts with the side-chain carboxylate. The same shift in the position of Arg292 was observed previously in the structure of a mutant AspAT complexed with aromatic substrate analogs (35). The most prominent effect of mutation of the two residues back to the wild type sequence on the substrate specificity is that ATBSN recovered the activity for dicarboxylic substrates (Table I and Fig. 1). On the other hand, the activity of ATBSN for β-branched substrates is decreased compared to that of ATB17. The shoulder above 500 nm observed in the absorption spectrum of ATB17 completely disappeared in the case of ATBSN (Fig. 2). This is consistent with the finding that the color of the purified ATB17 is orange while that of ATBSN or WT is yellow.

The most reasonable explanation for the above findings would be as follows: In ATB17, the β-hydroxyl group of the Thr142 side chain directly makes a van der Waals contact with the indole ring of Trp140. As a result, Trp140 is pushed against the pyridine ring of PLP. Enhanced π–π interaction between Trp140 and PLP would give rise to the absorption bands of ATB17 above 500 nm. The Ser139Gly mutation in ATB17 would increase the flexibility of the Pro138–Thr142 loop, enabling the backbone of the loop to change its conformation to release the structural strain caused by the Asn142Thr mutation. These adjustments widen the space above Trp140 and make it possible for the substrate binding pocket to accommodate the bulkier side chains of β-branched substrates. The hydrogen bond between Trp140 and the side chain of the dicarboxylic substrate cannot be formed in ATB17 because of the above conformational changes, which explain the decreased activity of ATB17 for dicarboxylic substrates.

The tertiary and quaternary structures of ATB17-isovalerate were significantly changed compared to those of the WT-maleate complex. Although the higher-order structure of the ATBSN-glutarate or ATBSN-succinate complex is similar to that of the WT-maleate complex, it is still not clear whether the structural difference between ATB17 and ATBSN (or WT) is caused by the two residues or by the difference in the bound analogs, because the structure of free ATB17 or that of the ATB17-dicarboxylic analog cannot be obtained

Substrate Specificity of ATBSN—The catalytic efficiency of ATBSN for glutamate or 2-oxoglutarate improved to the level of WT. In particular, the K_m values are smaller than those of WT (Table I). The turnover rate for the overall transamination reaction of ATBSN with aspartate and 2-oxovaline is smaller by about 100-fold than the value estimated from the rate constants for the half transamination reactions. This indicates that the rate-limiting step differs between the overall and half transamination reactions. The release of oxalacetate from the PMP form of ATBSN, the products of one of the two half transamination reactions comprising the overall reaction, may be the rate-limiting step in the overall transamination reaction. This idea is supported by the extremely high affinity of ATBSN for oxalacetate (K_m << 50 μM) or C4-dicarboxylic analogs (Table II). Thus, it is possible that the catalytic efficiency for aspartate or oxalacetate is also increased by the two mutations, although the kinetic parameters could not be determined experimentally.

As shown in Fig. 1, an aminotransferase, ATBSN, with a broad substrate specificity was unexpectedly obtained, which shows higher catalytic efficiencies for all the amino acid substrates than in the case of WT. The most characteristic feature of ATBSN is its small K_m values for the substrates, which is reflected in the small K_d values for analogs (Table II). Although this must be due to the influence of the other 15 substitutions, the mechanism through which the substrate binding is enhanced in the case of ATBSN remains to be elucidated.

Binding Mode of a C5-Dicarboxylic Analog—So far, no detailed analysis of the reaction of AspAT with glutamate has been performed, and thus there is no experimental evidence that the reaction with glutamate proceeds *via* the same reaction mechanism as that proposed for the reaction with aspartate. As for the glutamate-binding step, it is not clear if the enzyme structure is changed to a closed form or if the side chain carboxylate of glutamate interacts with Arg292 in the same way as that of aspartate does. To settle these long-standing controversies, several attempts have been made to determine the structures of the AspAT-C5 dicarboxylate complex (18–21). In those studies, (i) AspATs were cocrystallized with C4-dicarboxylic analogs and washed free of the analogs, and then the crystals were soaked in a solution containing C5-dicarboxylic ligands (18, 20); (ii) an apo AspAT was cocrystallized with 5′-phosphopyridoxyl glutamate (19), but the structure obtained does not necessarily represent the correct binding mode of glutamate because the glutamate moiety of this PLP derivative is forced into the substrate-binding site due to the high binding energy of its PLP moiety; and (iii) the PMP-form AspAT was cocrystallized with glutarate, but in this structure the C2 atom of glutarate is not located in a proper position to form an external Schiff base with the coenzyme, indicating the possibility that the complex is not a productive one (21). Because of the high affinity of ATBSN for glutamate and its analog (Tables I and II), we could cocrystallize it with glutarate and determine the structure of the complex that would reflect the productive Michaelis intermediate.

A comparison of the structures of the WT-maleate, ATBSN-succinate, and ATBSN-glutarate complexes (Figs. 3 and 4, B and C) revealed the following: First, the gross structures of the three complexes are almost identical. That is, the structure of the glutamate-bound enzyme, just like that of the aspartate-bound enzyme, is a closed form. Second, in all three structures, Arg292 interacts with the side-chain carboxylate group of the substrate analogs. As for the binding mode of a C5-dicarboxylic ligand, similar results

were previously obtained for the ketimine form of AspAT, that was obtained by soaking crystals of the PLP-form of AspAT in a solution containing glutamate (*20*). The findings in this study, although obtained for a mutant enzyme, support that AspAT binds glutamate and aspartate in a similar way and that the proposed reaction mechanism can also be applied to the reaction with glutamate.

REFERENCES

1. Velick, S.F. and Varva, J. (1962) A kinetic and equilibrium analysis of the glutamic oxalacetate transaminase mechanism. *J. Biol. Chem.* **237**, 2109–2122
2. Kiick, D.M. and Cook, P.F. (1983) pH studies toward the elucidation of the auxiliary catalyst for pig heart aspartate aminotransferase. *Biochemistry* **22**, 375–382
3. Jenkins, W.T. and Fonda, M.L. (1985) Kinetics, equilibria, and affinity for coenzymes and substrates in *Transaminases* (Christen, P. and Metzler, D.E., eds.) pp. 216–234, Wiley and Sons, New York
4. Kirsch, J.F., Eichele, G., Ford, G.C., Vincent, M.G., Jansonius, J.N., Gehring, H., and Christen, P. (1984) Mechanism of action of aspartate aminotransferase proposed on the basis of its spatial structure. *J. Mol. Biol.* **174**, 497–525
5. Malcolm, B.A. and Kirsch, J.F. (1985) Site-directed mutagenesis of aspartate aminotransferase from *E. coli*. *Biochem. Biophys. Res. Commun.* **132**, 915–921
6. Toney, M.D. and Kirsch, J.F. (1987) Tyrosine 70 increases the coenzyme affinity of aspartate aminotransferase. A site-directed mutagenesis study. *J. Biol. Chem.* **262**, 12403–12405
7. Kuramitsu, S., Inoue, Y., Tanase, S., Morino, Y., and Kagamiyama, H. (1987) Substitution of an arginyl residue for the active site lysyl residue (Lys258) of aspartate aminotransferase. *Biochem. Biophys. Res. Commun.* **146**, 416–421
8. Cronin, C.N. and Kirsch, J.F. (1988) Role of arginine-292 in the substrate specificity of aspartate aminotransferase as examined by site-directed mutagenesis. *Biochemistry* **27**, 4572–4579
9. Inoue, Y., Kuramitsu, S., Inoue, K., Kagamiyama, H., Hiromi, K., Tanase, S., and Morino, Y. (1989) Substitution of a lysyl residue for arginine 386 of *Escherichia coli* aspartate aminotransferase. *J. Biol. Chem.* **264**, 9673–9681
10. Ziak, M., Jäger, J., Malashkevich, V.N., Gehring, H., Jaussi, R., Jansonius, J.N., and Christen, P. (1993) Mutant aspartate aminotransferase (K258H) without pyridoxal-5′-phosphate-binding lysine residue. Structural and catalytic properties. *Eur. J. Biochem.* **211**, 475–484
11. Yano, T., Kuramitsu, S., Tanase, S., Morino, Y., and Kagamiyama, H. (1992) Role of Asp222 in the catalytic mechanism of *Escherichia coli* aspartate aminotransferase: the amino acid residue which enhances the function of the enzyme-bound coenzyme pyridoxal 5′-phosphate. *Biochemistry* **31**, 5878–5887
12. Borisov, V.V., Barisova, S.N., Kachalova, G.S., Sosfenove, N.I., and Vainshtein, B.K. (1985) X-ray studies of chicken cytosolic aspartate aminotransferase in *Transaminase* (Christen, P. and Metzler, D.E., eds.) pp. 155–164, Wiley and Sons, New York
13. Arnone, A., Rogers, P.H., Hyde, C.C., Briley, P.D., Metzler, C.M., and Metzler, D.E. (1985) Pig cytosolic aspartate aminotransferase: the structures of the internal aldimine, external aldimine, and ketimine and of the β subform in *Transaminases* (Christen, P. and Metzler, D.E., eds.) pp. 138–155, Wiley and Sons, New York
14. Kamitori, S., Okamoto, A., Hirotsu, K., Higuchi, T., Kuramitsu, S., Kagamiyama, H., Matsuura, Y., and Katsube, Y. (1990) Three-dimensional structures of aspartate aminotransferase from *Escherichia coli* and its mutant enzyme at 2.5 Å resolution. *J. Biochem.* **108**, 175–184
15. McPhalen, C.A., Vincent, M.G., and Jansonius, J.N. (1992) X-ray structure refinement and comparison of three forms of mitochondrial aspartate aminotransferase. *J. Mol. Biol.* **225**, 495–517
16. Okamoto, A., Higuchi, T., Hirotsu, K., Kuramitsu, S., and Kagamiyama, H. (1994) X-ray crystallographic study of pyridoxal 5′-phosphate-type aspartate aminotransferases from *Escherichia coli* in open and closed form. *J. Biochem.* **116**, 95–107
17. Kawaguchi, S. and Kuramitsu, S. (1998) Thermodynamics and molecular simulation analysis of hydrophobic substrate recognition by aminotransferases. *J. Biol. Chem.* **273**, 18353–18364
18. Harutynyan, E.G., Malashkevich, V.N., Kochkina, V.M., and Torchinsky, Y.M. (1985) Three-dimensional structure of the complex of chicken cytosolic aspartate aminotransferase with 2-oxoglutarate in *Transaminases* (Christen, P. and Metzler, D.E., eds.) pp. 164–173, Wiley and Sons, New York
19. Picot, D., Sandmeier, E., Thaller, C., Vincent, M.G., Christen, P., and Jansonius, J.N. (1991) The open/closed conformational equilibrium of aspartate aminotransferase. Studies in the crystalline state and with a fluorescent probe in solution. *Eur. J. Biochem.* **196**, 329–341
20. Malashkevich, V.N., Toney, M.D., and Jansonius, J.N. (1993) Crystal structures of true enzymatic reaction intermediate: Aspartate and glutamate ketimines in aspartate aminotransferase. *Biochemistry* **32**, 13451–13462
21. Miyahara, I., Hirotsu, K., Hayashi, H., and Kagamiyama, H. (1994) X-ray crystallographic study of pyridoxamine 5′-phosphate-type aspartate aminotransferases from *Escherichia coli* in three forms. *J. Biochem.* **116**, 1001–1012
22. Yano, T., Oue, S., and Kagamiyama, H. (1998) Directed evolution of an aspartate aminotransferase with new substrate specificities. *Proc. Natl. Acad. Sci. USA* **95**, 5511–5515
23. Oue, S., Okamoto, A., Yano, T., and Kagamiyama, H. (1998) Redesigning the substrate specificity of an enzyme by cumulative effects of the mutations of non-active site residues. *J. Biol. Chem.* **274**, 2344–2349
24. Yano, T., Kuramitsu, S., Tanase, S., Morino, Y., Hiromi, K., and Kagamiyama, H. (1991) The role of His143 in the catalytic mechanism of *Escherichia coli* aspartate aminotransferase. *J. Biol. Chem.* **266**, 6079–6085
25. Kuramitsu, S., Hiromi, K., Hayashi, H., Morino, Y., and Kagamiyama, H. (1990) Pre-steady-state kinetics of *Escherichia coli* aspartate aminotransferase catalyzed reactions and thermodynamic aspects of its substrate specificity. *Biochemistry* **29**, 5469–5476
26. Faesella, P., Giartosio, A., and Hammes, G.G. (1966) The interaction of aspartate aminotransferase with α-methylaspartic acid. *Biochemistry* **5**, 197–202
27. Fonda, M.L. and Johnson, R.J. (1970) Computer analysis of spectra of enzyme-substrate and enzyme-inhibitor complexes involving aspartate aminotransferase. *J. Biol. Chem.* **245**, 2709–2716
28. Higashi, T. (1990) Auto-indexing of oscillation images. *J. Appl. Crystallogr.* **23**, 253–257
29. Brünger, A.T., Kuriyan, J., and Karplus, M. (1987) Crystallographic R-factor refinement by molecular dynamics. *Science* **235**, 458–460
30. Engh, R.A. and Huber, R. (1991) Accurate bond and angle parameters for X-ray protein structure refinement. *Acta Crystallogr.* **A47**, 392–400
31. McRee, D.E. (1992) A visual protein crystallographic software system for X11/Xview. *J. Mol. Graphics* **10**, 44–47
32. Karmen, A. (1955) A note on the spectrophotometric assay of glutamic oxalacetate transaminase in human blood serum. *J. Clin. Invest.* **34**, 131–133
33. Jenkins, W.T. and Siezer, I.W. (1957) Glutamic aspartic transaminase. *J. Am. Chem. Soc.* **79**, 2655–2656
34. Kallen, R.K., Korpela, T., Martell, A.E., Matsushima, Y., Metzler, C.M., Metzler, D.E., Morozov, Y.V., Ralston, I.M., Savin, F.A., Torchinsky, Y.M., and Ueno, H. (1985) Chemical and spectroscopic properties of pyridoxal and pyridoxamine phosphates in *Transaminases* (Christen, P. and Metzler, D.E., eds.) pp. 37–108, Wiley and Sons, New York
35. Malashkevich, V.N., Onuffer, J.J., Kirsch, J.F., and Jansonius, J.N. (1995) Alternating arginine-modulated substrate specificity in an engineered tyrosine aminotransferase. *Nat. Struc. Biol.* **2**, 548–553